Journal of Taibah University Medical Sciences (2026) 21(4), 665–674

Taibah University

Journal of Taibah University Medical Sciences

www.sciencedirect.com

Original Article

Exploring drug repurposing for monkeypox virus: A structural and computational approach

Somia Gul, Ph.D. [a,*], Faiza Akhtar, M.Phil. [a,b], Iqra Rehman, M.Phil. [a], Muhammad Shah, M.Phil. [c], Umer Rashid, Ph.D [c] and Abdur Rauf, Ph.D [d]

[a] *Department of Pharmaceutical Chemistry, Faculty of Pharmacy, Jinnah University for Women, Karachi, Pakistan*
[b] *Department of Pharmaceutical Chemistry, Faculty of Pharmacy and Pharmaceutical Sciences, Ziauddin University, Karachi, Pakistan*
[c] *Department of Chemistry, COMSATS University Islamabad, Abbottabad Campus, Abbottabad, Pakistan*
[d] *Department of Chemistry, University of Swabi, Swabi, Pakistan*

Received 17 October 2025; accepted 11 June 2026; Available online 25 June 2026

الملخص

أهداف البحث: أدى التهديد العالمي المتزايد للعدوى الفيروسية المنتقلة من الحيوان إلى الإنسان إلى زيادة الاهتمام بالممرضات الناشئة مثل فيروس جدري القرود. هدفت هذه الدراسة إلى استكشاف إمكانية إعادة توظيف الأدوية بوصفها استراتيجية علاجية فعّالة ضد فيروس جدري القرود، مع التركيز على الارتباط الجيني الوثيق لهذا الفيروس بفيروسي الوقس والجدري.

طرق البحث: نظراً للتشابه البنيوي والتطوري بين فيروسات جنس الأورثوبوكس، تم اختيار دواء تيكوفيريمات، وهو دواء معتمد من هيئة الغذاء والدواء الأمريكية لعلاج الجدري، كدواء مرجعي. استُخدم نهج وصفي تحليلي لتقييم طاقات الارتباط لـ 38 دواءً معتمداً من هيئة الغذاء والدواء الأمريكية من أربع فئات علاجية. كما أُجري الالتحام الجزيئي ضد بروتينات مستهدفة رئيسية من جنس الأورثوبوكس، تلاه إجراء محاكاة الديناميكيات الجزيئية للتحقق من ثبات وتفاعلات أفضل معقدات الدواء والبروتين.

النتائج: أظهرت عدة مركبات ألفة ارتباط أقوى من الدواء المرجعي تيكوفيريمات، مما يشير إلى إمكانية إعادة توظيفها كعوامل مضادة لفيروس جدري القرود. وقد تضمنت المركبات الواعدة دارونافير، وسيميبريفير، وتيبرانافير، وإنديناڤير، وساكوينافير، وباريتابريفير، وإيداروبيسين، وغليكابريفير، حيث أظهرت درجات التحام جزيئي متفوقة مقارنة بالدواء المرجعي. كما دعمت محاكاة الديناميكيات الجزيئية ثبات هذه المعقدات الدوائية البروتينية واستمرار تفاعلاتها داخل المواقع النشطة للبروتينات المستهدفة، بما في ذلك الروابط الهيدروجينية والسلوك الديناميكي الملائم.

الاستنتاج: تقدم هذه الدراسة دلائل واعدة على إمكانية إعادة توظيف بعض الأدوية المعتمدة كمرشحات علاجية محتملة ضد فيروس جدري القرود. كما تدعم نتائج الالتحام الجزيئي ومحاكاة الديناميكيات الجزيئية جدوى هذه المركبات وثباتها، مما يعزز إمكانية تطوير تطبيقات علاجية جديدة قد تسهم في تحسين الاستجابة الصحية العامة وزيادة القيمة العلاجية والتجارية للأدوية المعاد توظيفها. ومع ذلك، تبقى الحاجة قائمة إلى دراسات تجريبية وسريرية إضافية للتحقق من فعاليتها وسلامتها ضد فيروس جدري القرود.

الكلمات المفتاحية: إعادة توظيف الأدوية؛ الأدوية المعتمدة من هيئة الغذاء والدواء الأمريكية؛ فيروس جدري القرود؛ فيروسات الأورثوبوكس

Abstract

Objective: The increasing global threat posed by viral infections that are transmitted to humans from animals has intensified interest in emerging pathogens such as monkeypox virus (MPV). This study investigated the potential of drug repurposing as an efficient therapeutic strategy against MPV, focusing on its close genetic relationships with vaccinia and variola viruses.

Methods: Due to the structural and evolutionary similarities among these orthopoxviruses, the Food and Drug Administration (FDA)-approved smallpox drug tecovirimat was selected as a reference drug. A descriptive-analytical approach was used to assess the binding energies of 38 FDA-approved drugs from four therapeutic classes. Molecular docking was performed against key target proteins from the genus *Orthopoxvirus*.

* Corresponding address: Department of Pharmaceutical Chemistry, Faculty of Pharmacy, Jinnah University for Women, Karachi, Pakistan.
E-mail: drsomi1983@yahoo.com (S. Gul)

Peer review under responsibility of Taibah University.

Production and hosting by Elsevier

1658-3612 © 2026 The Authors. Published by Elsevier B.V. This is an open access article under the CC BY-NC-ND license (http://creativecommons.org/licenses/by-nc-nd/4.0/). https://doi.org/10.1016/j.jtumed.2026.06.005

Results: Several compounds exhibited stronger binding energies than the reference drug tecovirimat, indicating their potential repurposing as anti-MPV agents. To further validate the stability and interaction dynamics of the top performing drug−protein complexes, molecular dynamics (MD) simulations were conducted, which supported their potential as viable candidates for future therapeutic development.

Conclusion: These findings provide promising leads for the development of new therapeutic applications, thereby enhancing both the public health response and commercial value of repurposed treatments. MD simulations also supported the stability and feasibility of these promising drug−protein complexes.

Keywords: Drug repurposing; FDA approved drugs; Monkeypox virus; Orthopoxviruses

© 2026 The Authors. Published by Elsevier B.V. This is an open access article under the CC BY-NC-ND license (http://creativecommons.org/licenses/by-nc-nd/4.0/).

Introduction

In the 21st century, zoonotic diseases have become a significant concern due to outbreaks with increased morbidity and mortality rates. Zoonotic diseases are infections that are transmitted between animals and human beings.[1] Outbreaks of SARS-CoV (2002−2003), MERS (2012), Ebola (2014−2016), and Nipah virus in recent decades highlight the increasing frequency and global threat posed by zoonotic infections.[2,3] The emergence of monkeypox in the first quarter of 2022 is a prime example of the rise of zoonotic diseases. This outbreak demonstrates the global threat posed by these viruses, which were previously considered endemic to specific regions, particularly Central and West Africa. However, recent outbreaks in the USA and Europe underscore the potential of zoonotic diseases to transcend geographical boundaries, evolving from endemic to pandemic threats.[2,3] Endemic and pandemic diseases are distinguished based on their spread and impact, where endemic diseases are consistently present in specific regions, whereas pandemic diseases can spread across multiple countries and continents, often causing widespread health crises. The outbreak of COVID-19 in the pandemic caused by SARS-CoV-2 virus is a recent example of how zoonotic diseases can escalate into a global health emergency, emphasizing the need for proactive measures to combat these threats.[4]

The monkeypox virus (MPV), vaccinia virus, and variola virus belong to the genus *Orthopoxvirus*, and share significant structural and genetic similarities. The vaccinia virus, historically used as a vaccine against smallpox, provides immunity against the variola virus, demonstrating the potential for cross protection among orthopoxviruses.[5] Monkeypox, a DNA virus, exhibits similar clinical symptoms to smallpox, including cutaneous lesions, fever, and lymphadenopathy, which distinguish it from other poxviruses.[6] The transmission of monkeypox occurs through animal bites, direct contact with infected animal fluids, or respiratory droplets, making it a significant public health concern.[6] Effective prevention of these infectious diseases involves vaccination and the treatment or control of closely related viruses, including smallpox. At present, no drug has been approved specifically for the treatment of monkeypox. Nevertheless, drug repurposing has developed as a promising new strategy to fill this gap. In drug repurposing, existing drugs are repurposed for new uses by identifying their therapeutic applications based on established safety profiles and pharmacological properties, allowing their development as treatments for emerging diseases.[7]

Drug repurposing is particularly advantageous for combating emerging infectious diseases such as monkeypox because it offers reduced timelines, lower risk of failure, and decreased costs,. For example, tecovirimat (TECO), an antiviral first developed for smallpox, was repurposed by the US Food and Drug Administration (FDA) and World Health Organization[8,9] for treating monkeypox under emergency use authorization. Similar to brincidofovir, its relative cidofovir exhibits antiviral activity against monkeypox infections, as shown by the Centers for Disease Control and Prevention.[10] Vaccinia immune globulin was adopted in KSA to treat monkeypox as a repurposed therapy, but its effectiveness has yet to be demonstrated.[11] Remdesivir was developed by Beigel et al.[12] to inhibit SARs-CoV-2 replication and was subsequently given emergency authorization for use in several countries.

Thalidomide, which was initially developed as a sedative and later withdrawn due to its teratogenic effects, was repurposed for the treatment of multiple myeloma, where its anti-angiogenic and immunomodulatory characteristics make it a valuable newly developed therapeutic for this type of cancer.[13] Ivermectin, an antiparasitic treatment for river blindness and other parasitic infections, has been investigated as a possible antiviral in an infectious disease context. Despite the controversial clinical effectiveness of ivermectin against COVID-19, it obtained promising results in the treatment of dengue and Zika.[14] Thus, the successful repurposing of drugs from existing pharmacopeias is highlighted by the usefulness of implementing repurposed drug strategies during public health emergencies.

Recently, computational methods have revolutionized drug discovery and repurposing efforts. *In silico* techniques, such as molecular docking and virtual screening, enable researchers to predict drug−receptor interactions with high accuracy, significantly reducing the time and cost associated with experimental validation.[15] For example, computational studies have identified several FDA-approved drugs, such as antibacterial and anticancer agents, as potential candidates for drug repurposing.[16−18] Combining computational and experimental methods can accelerate the development of effective treatments for emerging zoonotic diseases and minimize their impacts on global health.

Thus, drug repurposing is a fundamental basis for addressing the most urgent critical therapeutic requirements for new zoonotic diseases, including monkeypox. Drug repurposing is a viable solution to the problem of emerging infectious diseases, ultimately reducing the time required to develop efficient treatments through the best use of

information about known drugs, as well as using innovative technologies and emerging zoonotic treatments, thereby preserving public health.

The present study explored the critical role of drug repurposing as a rapid and cost effective strategy for combating emerging zoonotic diseases, particularly by focusing on monkeypox. By utilizing computational advances in repurposed therapeutics, we aimed to highlight how leveraging existing pharmacopeias can accelerate drug development, mitigate global health crises, and establish a robust framework for addressing future outbreaks. Ultimately, in this study, we aimed to contribute to the evolving landscape of infectious diseases management by promoting innovative idea-driven approaches to drug discovery and deployment.

Materials and methods

Software for molecular docking

In silico investigations were conducted by utilizing an Intel Core i7 processor with 2.90 Ghz, 8 GB RAM, and the Windows 10 Pro operating system. Molecular docking studies were performed using AutoDock (version 4.2.6) and AutoDock tools (version 1.5.7). The resulting docked complexes were evaluated with PyMOL (version 2.3.2). ChemDraw professional (version 17.1) was employed for depicting ligand structures. Ligand energy minimization was conducted by using CHEM 3D Ultra. Furthermore, the visualization and preparation of proteins were facilitated by BIOVIA Discovery Studio Visualizer. Molecular dynamics (MD) simulations were conducted by using GROMACS software.

Methods

A descriptive-analytical approach was employed to investigate the molecular interactions between selected FDA-approved compounds and target proteins belonging to the genus *Orthopoxvirus* within the Poxviridae family.[19] In total, 38 FDA-approved drugs were chosen for evaluation, representing four pharmacological categories, i.e., antivirals, anthracyclines, antiretroviral HIV-1 protease inhibitors, and hepatitis C virus (HCV) NS3/4A protease inhibitors, for repurposing in MPV treatment.

Target proteins were selected based on their relevance to the pathogenicity of *Orthopoxvirus* and structural availability in Protein Data Bank (PDB). The viral target proteins included: thymidylate kinase from vaccinia virus (PDB ID: 2V54), A42R protein from MPV (PDB ID: 4QWO), a structural protein from vaccinia virus (PDB ID: 7SEZ), and methyl transferase VP39 from MPV (PDB ID: 8B07).

Given the close genetic and structural similarities between MPV and variola virus, an FDA-approved antiviral agent for smallpox, TECO, was included as a reference compound for comparative analysis.[20]

Retrieval of targets and ligands from databases

The PubChem database was used to obtain structural information for selected compounds (ligands).[21] The structures were retrieved in SDF format and then converted into PDB format. The three-dimensional structures of selected target proteins were retrieved from PDB.[22] The target proteins were selected based on the close structural associations of MPV with vaccinia virus and variola virus. Hence, the first protein target was the crystal structure of vaccinia virus with thymidylate kinase bound to thymidine diphosphate (PDB ID: 2V54, resolution: 2.4 Å).[23] The second target protein was the crystal structure of MPV methyltransferase VP39 in complex with sinefungin (PDB ID: 8B07, resolution: 2.05 Å).[24] The third target protein retrieved from PDB was the crystal structure of vaccinia virus decapping enzyme D9 in complex with 7-Methylguanosine 5'-diphosphate (7GDP) (PDB ID: 7SEZ, resolution: 1.70 Å).[25] The final target protein was the crystal structure of A42R profilin-like protein from MPV Zaire-96-1-16 (PDB ID: 4QWO, resolution: 1.52 Å).[26] The target protein structures were prepared by using BIOVIA Discovery Studio Visualizer, which involved various steps such as deleting all water molecules, hetero atoms, and adding hydrogen atoms. The new files were saved in PDB format for docking analysis.

Docking by virtual screening

To explore the molecular interactions between different selected compounds and the target proteins of MPV, molecular docking by virtual screening was conducted with AutoDock Vina,[27] which involved generating a virtual combinatorial library of clinically approved compounds. Energy minimization was performed for each compound in the virtual combinatorial library to optimize its geometry by utilizing MMFF94 in CHEM 3D Ultra.[28] After the addition of charges and polar hydrogen, all of the PDB files for ligands and targets were converted into PDBQT files. Centroid grid boxes were generated to specify the active sites. The docking parameters, including orientation and torsion angles (7.5), number of generations (27,000), and energy evaluations (250,000), were set to the default values. The predicted binding energies and best conformations of the docked structures were utilized to rank the complexes formed by ligands and target proteins.

Screening criteria

The aim of the current study was to identify the most suitable ligand candidates capable of forming stable and strong interactions with target proteins from the genus *Orthopoxvirus*, particularly by focusing on MPV. Docking was conducted by using AutoDock for screening the binding energies and interaction profiles of selected FDA-approved drugs with the viral targets. PyMOL and Discovery Studio Visualizer tools were utilized to visualize and analyze the outcomes of molecular docking.

MD simulations of ligand–protein complexes

After docking analysis, the selected complexes were further investigated by conducting MD simulations using GROMACS software. The stabilities of proteins before and after complexation, structural dynamics, and interactions

with ligands were investigated under natural body conditions through MD simulations. The stability of each ligand with the active site was also analyzed. The MD simulations involved generating the cubic shape box, followed by solvation with the TIP3P water model. After solvation, the protein was neutralized using sodium and chlorine salt. The system was minimized in 5000 steps, followed by two steps of NPT (constant Number of particles, Pressure, and Temperature) and NVT (constant Number of particles, Volume, and Temperature) equilibration at the optimum level (1 atm, 310.15 K). After applying natural body conditions, the system was simulated up to 100 ns. Post-MD treatment was executed by conducting three types of analysis: root mean square deviation (RMSD), root mean square fluctuation (RMSF), and hydrogen bonding (HB) histogram interaction analysis.

Results and discussion

The ongoing spread of MPV demands the immediate development of an effective therapeutic solution. New antiviral drug development is a lengthy and resource-intensive process, so repurposing existing FDA-approved drugs is a suitable strategy for obtaining practical and time-efficient solutions. Molecular docking methods were used to analyze 38 approved therapeutic drugs as potential MPV protein inhibitors that target thymidylate kinase (PDB ID: 2V54), methyltransferase VP39 (PDB ID: 8B07), decapping enzyme D9 (PDB ID: 7SEZ), and profilin-like protein A42R (PDB ID: 4QWO). Molecular connectivity data regarding drug interactions with MPV proteins were successfully obtained to highlight their potential inhibitory effects and suitability for further investigation.

Molecular docking studies

The 38 selected FDA-approved drug candidates and reference drug TECO were investigated in molecular docking studies by using AutoDock Vina to evaluate four protein targets and their docked positions with the lowest binding energies, as shown in Table 1, which presents the names of the 38 drugs and their codes.

The docking results for vaccinia virus thymidylate kinase (PDB ID: 2V54) indicated that the binding affinities varied among the 38 FDA-approved drugs from four pharmacological classes: antivirals, anthracyclines (anticancer agents), antiretroviral HIV-1 protease inhibitors, and HCV NS3/4A protease inhibitors. TECO, an FDA-approved antiviral, was used as a reference in this study and it had a binding energy of −7.5 kcal/mol, and it was applied as a standard for evaluating the performance of other ligands.

The strongest binding interactions were observed with compounds from the antiretroviral HIV-1 protease inhibitor class, where saquinavir (SAQU) had the lowest binding energy of −9.5 kcal/mol, followed closely by indinavir (INDI) with −9.4 kcal/mol. These values were significantly lower than that for TECO, suggesting their superior binding energy and stronger interaction with the 2V54 target. Other strong binding energies in this class included lopinavir (LOPI) with −8.6 kcal/mol, tipranavir (TIPR) with −8.2 kcal/mol, and darunavir (DARU) with −7.9 kcal/mol.

The HCV NS3/4A protease inhibitors also yielded promising results, including glecaprevir (GLEC) with −8.9 kcal/mol, simeprevir (SIME) with −8.7 kcal/mol, and paritaprevir (PARI) with −8.6 kcal/mol, which all outperformed TECO. In addition, asunaprevir (ASUN) with −7.7 kcal/mol and telaprevir (TELA) with −7.2 kcal/mol had moderate binding energies compared with the reference.

Among the anthracycline class of anticancer agents, doxorubicin (DOXO) and epirubicin (EPI) both had binding energies of −7.1 kcal/mol, which were slightly less than that for TECO but still indicative of potentially useful interactions. Idarubicin (IDAR) with −7.0 kcal/mol and daunorubicin (DANU) with −6.7 kcal/mol also had similar binding energies.

By contrast, most of the antiviral agents had binding energies in the range of −4.5 to −6.3 kcal/mol, and weaker compared with TECO.

Notably, SAQU, INDI, GLEC, and SIME emerged as strong candidates for repurposing against MPV based on the results against the target vaccinia virus thymidylate kinase (PDB ID: 2V54).

Against the MPV VP39 protein (PDB ID: 8B07), PARI had the strongest binding energy of −9.0 kcal/mol, and those for other drugs included GLEC with −8.7 kcal/mol, IDAR with −8.6 kcal/mol, sofosbuvir (SOFO) with −8.4 kcal/mol, and SIME with −8.3 kcal/mol. These drugs are mainly HCV inhibitors and anthracyclines, and they may have high potential for repurposing against MPV.[29]

Against vaccinia virus protein (PDB ID: 7SEZ), the compounds with the best binding energies were DARU with −10.6 kcal/mol, TIPR with −10.1 kcal/mol, and SAQU, LOPI, and nelfinavir (NELF) with −10.0 kcal/mol. Atazanavir (ATAZ) and SIME both had binding energies of −9.7 kcal/mol. These HIV-1 and HCV protease inhibitors had better binding energies than the standard TECO with −7.5 kcal/mol, thereby highlighting their strong binding potential for repurposing against MPV.

For the MPV A42R protein (PDB ID: 4QWO), several drugs had stronger binding energies than the reference drug TECO with 9.3 kcal/mol. Among the HCV NS3/4A protease inhibitors, PARI with −10.4 kcal/mol and SIME with −10.3 kcal/mol had the highest binding energies, indicating their excellent potential for repurposing within this class. GLEC with −9.3 kcal/mol had the same binding energy as TECO, as shown in Table 1.

Molecular docking analysis provided useful insights into the binding energies of selected drug candidates with four target proteins: 2V54, 8B07, 7SEZ, and 4QWO. Among all of the drug candidates, DARU achieved the highest binding energy with −10.6 kcal/mol against 7SEZ, followed by SIME with −10.3 kcal/mol and TIPR with −10.1 kcal/mol. The drug candidates INDI and SAQU had stronger binding energies of −9.5 kcal/mol and −9.4 kcal/mol, respectively, against 2V54 compared with the reference drug TECO (−7.5 kcal/mol). PARI had a binding energy of −9.0 kcal/mol against 8B07, followed by IDAR with −8.6 kcal/mol. Against 4QWO, SIME had a binding energy of −10.3 kcal/mol and GLEC had a binding energy of −9.3 kcal/mol.

The standard drug TECO had moderate binding energies with all targets ranging between −7.5 and −9.3 kcal/mol. The results indicated that PARI, SAQU, and GLEC had high binding energies, making them potential candidates for

Table 1: Docking results with FDA-approved drugs for repurposing against MPV.

Drug code	Drug name	Molecular wt. (g/mol)	Energy min. (kcal/mol)	Binding energy with selected target proteins			
				2V54	8B07	7SEZ	4QWO
TECO	Tecovirimat (standard)	376.3	46.6858	−7.5	−8.9	−7.5	−9.3
Antivirals							
ABAC	Abacavir	286.34	−49.8031	−5.7	−7.4	−5.1	−4.9
ACY	Acyclovir	225.20	−40.15	−6.3	−6.5	−4.9	−5.4
ADE	Adefovir	273.19	−44.616	−5.4	−5.7	−4.9	−5.2
CIDO	Cidofovir	279.19	−103.371	−4.6	−6.3	−5.1	−5.5
DIDA	Didanosine	236.23	29.9368	−5.2	−7.7	−6.0	−5.5
EMT	Emtricitabine	247.25	−24.5241	−4.8	−6.7	−5.4	−5.0
ENTE	Entecavir	277.28	−22.1713	−4.5	−7.4	−6.5	−6.4
FAMI	Famciclovir	321.33	−78.4286	−4.7	−6.8	−5.6	−4.6
GANC	Ganciclovir	255.23	−23.4015	−5.3	−6.7	−5.6	−5.8
LAMI	Lamivudine	229.26	−58.9077	−4.8	−6.5	−5.3	−4.9
REMD	Remdesivir	602.6	1.0189	−6.1	−7.6	−7.3	−5.6
SOFO	Sofosbuvir	529.5	−104.153	−6.2	−8.4	−6.3	−5.6
STAV	Stavudine	224.21	−79.843	−5.7	−7.6	−6.2	−5.5
TELB	Telbivudine	242.23	−62.2787	−5.8	−7.7	−6.1	−5.7
TENO	Tenofovir	287.21	−41.9011	−5.8	−6.7	−5.1	−5.5
VALA	Valacyclovir	324.34	−2.69927	−4.8	−7.2	−5.6	−5.9
ZIDO	Zidovudine	267.24	−78.6322	−5.3	−7.4	−6.4	−5.8
Anthracyclines							
DANU	Daunorubicin	527.5	124.124	−6.7	−6.4	−7.6	−6.4
DOXO	Doxorubicin	543.5	139.885	−7.1	−6.0	−7.4	−6.0
EPI	Epirubicin	543.5	138.005	−7.1	−6.2	−7.5	−6.2
IDAR	Idarubicin	497.5	121.948	−7.0	−8.6	−7.7	−6.5
Antiretroviral HIV−1 protease inhibitors							
AMP	Amprenavir	505.6	−3.2309	−7.6	−7.1	−9.0	−7.7
ATA	Atazanavir	704.9	105.499	−7.3	−7.0	−9.7	−7.9
DARU	Darunavir	547.7	−13.0482	−7.9	−6.8	−10.6	−7.0
FOSA	Fosamprenavir	585.6	−213.689	−6.8	−7.0	−8.3	−7.7
INDI	Indinavir	613.8	190.936	−9.4	−7.4	−9.0	−8.4
LOPI	Lopinavir	628.8	41.7214	−8.6	−7.7	−10.0	−7.5
NELF	Nelfinavir	567.8	118.052	−7.2	−7.4	−10.0	−8.5
RITO	Ritonavir	720.9	−34.185	−6.6	−7.7	−9.1	−7.3
SAQU	Saquinavir	670.8	156.352	−9.5	−7.3	−10.0	−8.8
TIPR	Tipranavir	602.7	118.398	−8.2	−6.1	−10.1	−8.4
Hepatitis C virus NS3/4A protease inhibitors							
ASUN	Asunaprevir	748.3	118.398	−7.7	−8.0	−8.4	−7.7
BOCE	Boceprevir	519.7	43.6946	−5.9	−5.9	−6.8	−7.3
GRAZ	Grazoprevir	766.9	51.7657	−6.7	−7.9	−7.8	−8.5
PARI	Paritaprevir	765.9	1410.43	−8.6	−9.0	−9.4	−10.4
GLEC	Glecaprevir	838.9	65.7389	−8.9	−8.7	−7.1	−9.3
SIME	Simeprevir	749.9	8.84494	−8.7	−8.3	−9.7	−10.3
TELA	Telaprevir	679.8	216.187	−7.2	−7.1	−8.0	−8.5

further evaluation. Thus, our results suggest that these compounds have potential uses as inhibitors for multiple target proteins in MPV as they exhibited selective behavior against certain targets. The best selected compounds are listed in Table 2.

Binding interactions with hydrophobic and hydrophilic residues

In the present study, we identified key amino acids that played strong roles in facilitating drug−protein binding by forming hydrogen bonds and hydrophobic interactions, as shown in Table S1. Against the target protein (PDB ID: 2V54), SAQU formed strong hydrogen bonds at ARG-41(2.1 Å) and ASP-13 (2.3 Å), as well as forming hydrophobic bonds with MET-22 (3.6 Å) and GLN-40 (3.3 Å). The strength of thymidylate kinase inhibition by this compound increased its possible function as a potent antiviral agent through these protein−drug interactions. Similarly, against the target protein (PDB ID: 2V54), INDI formed two hydrogen bonds at ARG-137 (2.5 Å) and ARG-41 (2.3 Å), as well as hydrophobic interactions at GLY-16 (3.4 Å) and TYR-35 (2.6 Å) (Figure 1). These molecular interactions between INDI and the target protein demonstrate that it can effectively inhibit MPV replication by targeting fundamental enzymatic sites.

TECO established stable bonding interactions between TYR-189 and the target protein 8B07 to form two hydrogen

Table 2: Best selected drugs with strong binding energies for repurposing against MPV.

Drug code	Binding energy with selected target proteins			
	2v54	8B07	7SEZ	4QWO
TECO	−7.5	−8.9	−7.5	−9.3
INDI	−9.4			
SAQU	−9.5			
PARI		−9.0		
IDRA		−8.6		
DARU			−10.6	
TIPR			−10.1	
SIME				−10.3
GLEC				−9.3

bonds with bond lengths of 2.6 Å and 3.6 Å, and further stabilized its binding with hydrophobic contacts with PHE-115 at 4.2 Å and ARG-97 at 4.1 Å. With the same protein target, PARI engaged in strong binding through PHE-293 (3.8 Å) and ASN-273 (4.1 Å), and formed hydrophobic interactions with LYS-274 (4.0 Å) Fig. S1. These interactions demonstrate the significant inhibitory potential of TECO and PARI against their designated targets.

Against the target protein 7SEZ, the DARU complex formed numerous interactions with four hydrogen bonds at ARG-50 (2.4 Å), HIS-33 (3.0 Å), GLU-130 (2.6 Å), and LYS-198 (2.2 Å), as well as an additional hydrophobic interaction at TYR-158(2.3 Å). The hydrogen bonds in TIPR (PDB ID: 7SEZ) connected HIS-33 with bond lengths of 2.3 Å and 2.6 Å, and another hydrogen bond was observed with ARG-50 (3.1 Å). The drug TIPR also stabilized through hydrophobic bond interactions at GLN-57 (2.5 Å) Fig. S2. These interactions show that DARU and TIPR can successfully disrupt the viral protease functions that are required for the virus to survive.

The binding interactions between SIME and the target protein 4QWO included hydrogen bonds with LYS-26 (2.1 Å, 2.4 Å) and LYS-29 (2.5 Å), and a hydrophobic bond with HIS-100 (3.2 Å). Against the same target protein, GLEC formed hydrogen bonds through SER-12 with bond lengths of 2.4 Å and 2.5 Å, as well as another hydrogen bond with ARG-38 (2.8 Å) and hydrophobic interactions with ILE-35 (3.6 Å) Fig. S3. The drug−protein interactions contributed to their binding strength and reinforced their ability to function as effective inhibitors. The ability of these drugs to establish multiple hydrogen bonds and hydrophobic interactions enhances their stability within viral active sites, possibly playing crucial roles in disrupting the key processes essential for MPV replication.[17]

Based on the docking analysis results, the drug candidates that can potentially be repurposed against MPV (see Table 2) were further tested in MD simulations. The drugs were selected based on their binding energies as well as steady hydrogen bond interactions and hydrophobic bonds within the active sites. We prioritized drugs that formed robust molecular bonds with key amino acid positions in the active site. The drugs that passed the selection stage had the best docking scores when assessed against all four proteins, and they also belonged to different drug classes. The selected candidate molecules were assessed in MD simulations to validate their potential inhibitory activities, as well as to evaluate their stability and adaptability to changing biological environments.

MD simulations

DARU complex

Following docking analysis, the selected protein−ligand DARU complex was further studied through MD simulations using GROMACS software. The structural and dynamic changes in the protein were analyzed based on RMSD plots, RMSF plots, and HB histograms. The results showed that RMSD was within 0.15−0.35 nm. However, the complex RMSD plot had a greater deviation compared with the protein, where the deviation started at 20 ns and the stable nature of the RMSD changed after 50 ns. The RMSF graph showed that both the protein and protein−ligand complexes exhibited the same fluctuating pattern, with different intensities. Overall, the protein−ligand complex fluctuated more than the protein, which indicated the presence of the ligand within the active site. The highest fluctuations for the DARU complex were observed in various regions, including the 60−80 and 110−140 regions. The higher functions of the protein compared with the DARU complex were observed in the 20−40 and 90−100 regions. The most important parameter for the protein−ligand complex was the HB histogram, which showed that the protein and ligand interacted through a HB range of 2−6. During the starting frames, the complex contained six hydrogen bonds, which slowly decreased to two hydrogen bonds, as shown in Figure 2.

GLEC complex

The GLEC complex was also analyzed through MD simulations under natural body conditions. The RMSD plots for the protein and protein−ligand complex showed that the protein exhibited almost stable behavior within 2.0−2.5 nm, with some variations only in the first 20 ns and a range of 1.5−2.5 nm. After ligand inhibition, the RMSD increased for the complex, where it increased with time, starting at 2.0 nm and ending at 3.0 nm. This change in behavior indicated the effect of the ligand on the protein. The RMSF plot showed the mixed behavior of different parts of the GLEC complex during the simulation. The RMSF was mostly higher for the complex than the protein, including at 10−20, 25−35, and 40−50 nm, but the RMSD was lower for the complex than the protein at 50−65 nm. The HB histogram demonstrated that HB ranged from two to five bonds. HB was low in the starting 250 frames, but the complex subsequently had more than three hydrogen bonds, as shown in Fig. S4.

SAQU complex

MD simulations were performed for the protein−ligand docking complexes to investigate the binding stability and intermolecular interactions within a reference period. The stability and intermolecular contacts between the proteins and molecules were confirmed in MD simulations to examine the complex docking file for the topmost compound over a time interval of 100 ns. The MD trajectories were retrieved, and the simulation results were assessed using RMSD, RMSF, and HB analysis.

In the MD simulations, the RMSD was used to calculate the average distance obtained by atom displacement for a given reference time frame. It was possible to detect whether

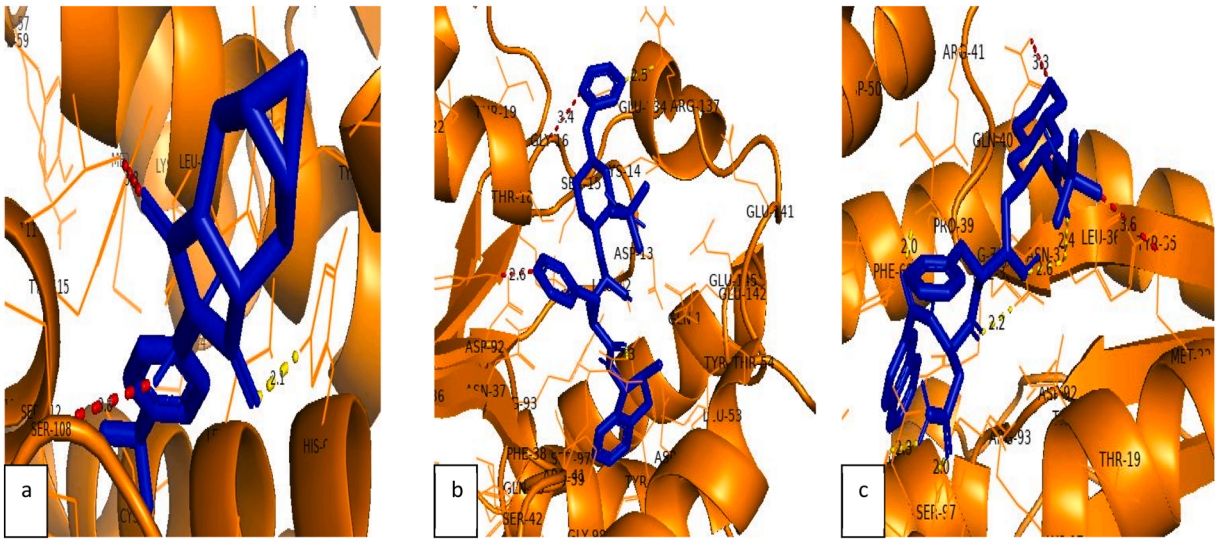


Figure 1: Hydrogen bonding (yellow) and hydrophobic bonding (red) interactions with: (a) TECO, (b) INDI, and (c) SAQU at the active site of the target 2V54.

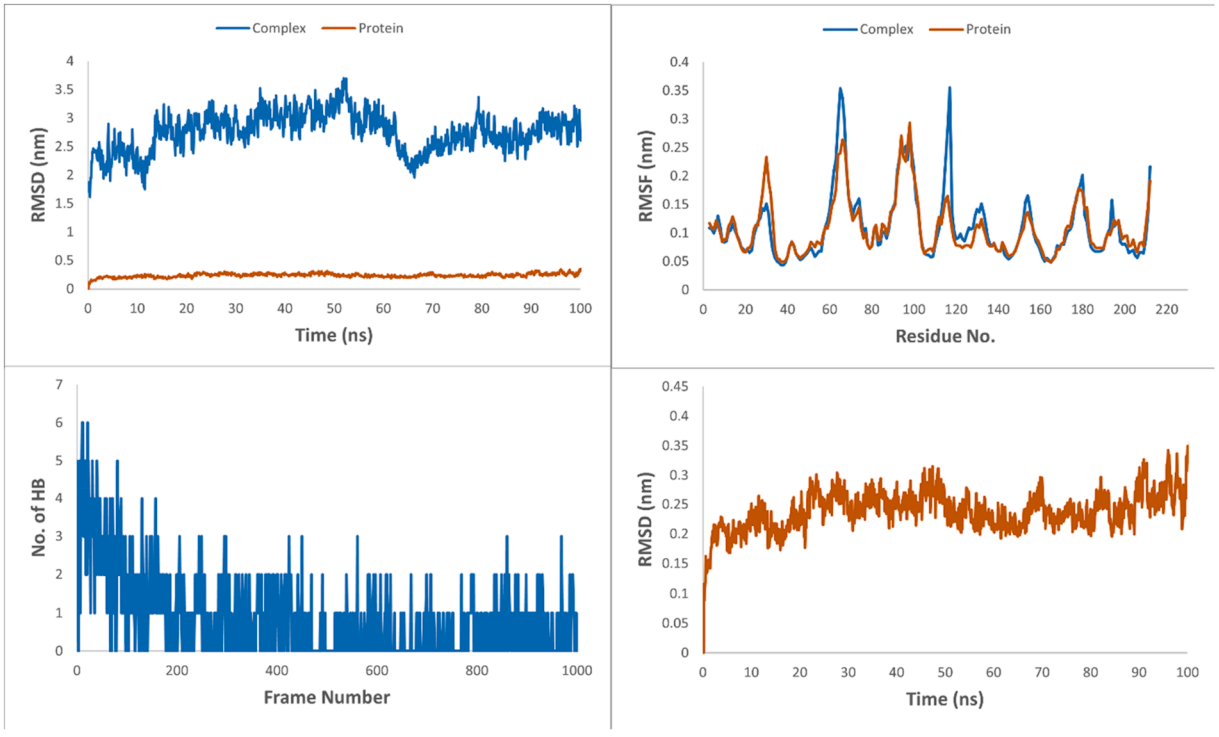


Figure 2: RMSD plot, RMSF plot, and HB histogram for DARU complex (blue = protein–ligand complex, brown = protein).

the simulation had equilibrated based on the RMSD result. The backbone deviation (N, Cα, C) of the protein was derived using the RMSD value obtained from the MD simulation. The complex structure exhibited minor fluctuations (1–2%) at 1.6–2.2 nm for 53–75 ns until reaching equilibrium. Immediately following equilibration at 2–2.2 nm, the system became stable, and this then tended to be maintained for up to 100 ns, or from 75 to 100 ns. The average RMSD for the protein–ligand complex was 1.3 nm, and the fluctuations were also within acceptable limits. The protein fluctuated at 2.5 nm for 41 ns until reaching equilibrium. The protein reached equilibrium at 1.6 nm for 43 ns and continued up to 100 ns. The average RMSD value for the protein was 1.6 nm, which is acceptable. Fluctuations between 1 and 3 nm within a reference protein structure are entirely normal; however, considerably greater values show that the protein has undergone significant conformational change and that the system is no longer stable.

The RMSF plot was required to determine and characterize the local conformational changes in the protein chain

and ligand. Due to intermolecular interactions between the ligand and receptor, small fluctuations were observed in the protein–ligand complex; however, the highest fluctuations were observed in the region where residues formed hydrophobic interactions with the ligand. The results showed that the RMSF plots for the protein and protein–ligand complex were very similar to each other and below 0.4 nm, with few exceptions. The RMSF value sharply decreased from 0.35 to 0.05 nm at the beginning. A clear deviation in the RMSF for the complex compared with the protein was observed in amino acid residues ranging from 30 to 70. Another deviation was observed around the 90–100 range. A third deviation was observed in the region of 180.

The simulations indicated the formation of hydrogen bonds with sufficient frequencies throughout the simulation. HB analysis is very important for understanding protein–ligand interactions. The results showed that the synthesized compound interacted with proteins at a HB frequency of 1–5. The inhibitor mostly had one, two, and three hydrogen bonds. The compounds had three and four hydrogen bonds in some cases, as shown in Fig. S5.

SIME complex

The structural dynamics of the SIME protein–ligand complex were studied for 100 ns in MD simulations. The RMSD plots showed that the protein and protein–ligand complex exhibited the same behavior during the first 50 ns with different levels of deviation. The deviation started at 1 nm for the complex and at 1.7 for the protein, and the difference in the RMSD remained equal for the first 50 ns, indicating the stability of the complex after ligand inhibition. After 50 ns, the RMSD deviation for the protein was in the same region and slightly higher than that for the complex. The RMSF plot indicated a high level of similarity based on the fluctuating movements of residues with different intensities. The highest fluctuation of 0.4 in the complex was observed between 70 and 80, and another clear difference was observed at 35–45. The HB histogram showed that the maximum number of hydrogen bonds was three, with a single hydrogen bond in most of the frames. There were two hydrogen bonds in the first half and one in the second half, as shown in Fig. S6.

SAQU complex

MD simulations were performed for protein–ligand docking complexes to investigate the binding stability and intermolecular interactions within a reference period. The stability and intermolecular contacts between proteins and molecules were confirmed using MD simulations to examine the complex docking file for the topmost compound over a time interval of 100 ns. The MD trajectories were retrieved and the simulation results were assessed using RMSD, RMSF, and hydrogen bond analysis.

In the MD simulations, the RMSD was used to calculate the average distance obtained by atom displacement for a given reference time frame. It was possible to detect if the simulation had equilibrated based on the RMSD plot. The backbone deviation (N, Cα, C) of the protein was derived using the RMSD value obtained from the MD simulations. The complex structure was subjected to minor fluctuations at 2–2.5 nm for 20–30 ns until reaching equilibrium. Immediately following equilibration at 2–3 nm, the system became stable, and tended to be maintained for up to 100 ns. The average RMSD for the protein–ligand complex was 2.3 nm, and the fluctuations were also within acceptable limits. The protein fluctuated at 0.12 nm for 30–43 ns until reaching equilibrium. The protein reached equilibration at 0.3–0.15 nm for 43 ns and continued up to 100 ns. The average RMSD value for the protein was 0.3 nm, which is acceptable.

The RMSF plot was required to determine and characterize the local conformational changes in the protein chain and ligand. Due to intermolecular interactions between the ligand and the receptor, small fluctuations were observed in the protein–ligand complex. However, the greatest fluctuations were observed in the region where residues formed hydrophobic interactions with the ligand. The results showed that the RMSF plots for the protein and protein–ligand complex were very similar to each other and below 0.4 nm, with few exceptions. The RMSF value sharply decreased from 0.35 to 0.05 nm at the beginning. A clear deviation between the RMSF for the complex and that for the protein was observed in amino acid residues ranging from 40 to 70. Another deviation was observed around the range from 130 to 160.

The simulation demonstrated the formation of hydrogen bonds with sufficient frequencies throughout the simulation. HB analysis is very important for understanding protein–ligand interactions. The results showed that the synthesized compound interacted with the protein at a HB frequency of 1–10. The inhibitor mostly had one, two, and three hydrogen bonds, with four, five, and six hydrogen bonds in some cases, as well as a few with seven to 10 hydrogen bonds in others, as shown in Fig. S7.

TECO 4QWO complex

The TECO 4QWO complex was also simulated in further analysis. The RMSD plot showed that the protein exhibited almost stable behavior during 100 ns in the MD simulation, with a deviation between 0.1 and 0.15 nm. After ligand binding, the RMSD plot for the complex increased and the deviation started between 1 and 2 nm during the simulation. There was only one sharp change at 40 ns. Overall, the complex exhibited stable behavior. The RMSF plots for the TECO 4QWO complex and protein had the same fluctuating pattern and high similarity, with one exception from residue numbers 35–60. The complex exhibited greater fluctuations at 0.1–0.3 nm, which indicated the influence of the ligand on that region of the protein. The RMSF plot showed that the amino acid residues after 60 remained stable in the protein after complex formation. The HB histogram for the TECO 4QWO complex showed that the number of hydrogen bonds ranged between 1 and 3 throughout the simulation, with an average of two hydrogen bonds. There were more HB interactions in the last 500 frames than the first half, as shown in Fig. S8.

TIPR complex

The TIPR protein–ligand complex was selected for further exploration in MD simulations. The RMSD plot for the protein indicated stable behavior (with a variation between 0.2 and 0.3 nm) compared with the complex during the MD simulation for 100 ns. After ligand binding with the protein, the dynamics changed and the variation increased. For the complex, the RMSD deviated at a low level below 2 nm up to 20 ns until a conformational change occurred after 20 ns and the deviation

started at more than 3 nm up to 100 ns. The RMSF plot exhibited the same fluctuating pattern across the backbone of the protein with variations in the intensities. The complex mostly exhibited greater fluctuations than the protein, which indicated the influence of the ligand on the protein. In the complex, the residues between 25 and 35, 55−70, 175−185, and 190−205 had slightly greater fluctuations, but the residues from 110 to 120 and the last 10 residues exhibited the highest fluctuations. The HB histogram for the TIPR complex showed an interaction through a single hydrogen bond throughout the MD simulation, with two HB interactions in some cases, as shown in Fig. S9.

Conclusion

The resurgence of MPV is a global health concern that highlights the critical need to rapidly identify effective antiviral therapeutics. In this study, we systematically employed molecular docking and MD simulations to evaluate the inhibitory potential of 38 FDA-approved drugs from various classes, i.e., HCV NS3/4A protease inhibitors, antiretroviral HIV-1 protease inhibitors, anticancer drugs, and antivirals, against four key orthopoxvirus protein targets. The results showed that DARU, SIME, TIPR, INDI, SAQU, PARI, IDAR, and GLEC had superior docking scores, indicating their potential use as better broad-spectrum antiviral candidates compared with the reference drug TECO. These findings support the feasibility of drug repurposing for MPV treatment. MD simulations conducted under physiological conditions further validated the docking results by confirming the structural stability and sustained interactions. The MD simulations showed that the ligands remained stably bound within the active sites of their targets, and they exhibited consistent HB and favorable dynamic behavior over time. These results supported the reliability of the docking predictions and highlight the potential repurposing of the selected compounds as stable and effective inhibitors of MPV proteins.

Source of funding

This research did not receive any specific grants from funding agencies in the public, commercial, or not-for-profit sectors.

Conflict of interest

The authors declare that they have no known conflicts of interest, competing financial interests, or personal relationships that could have appeared to influence the work reported in this paper.

Ethical approval

This study did not include any animal or human subjects, so ethical approval was not required.

Authors' contributions

SG: Conceptualization, Validation, Writing - Review & Editing, Supervision, Project administration. FA: Conceptualization, Methodology, Formal analysis, Investigation, software, Writing - Original Draft. IR: Methodology, software, Resources, Visualization, Data Curation, Writing - Original Draft, Investigation. MS: Methodology, software, Visualization, Resources. UR: Investigation, software, Resources, Visualization, Writing - Review & Editing. AR: Investigation, Formal analysis, Resources. All authors have critically reviewed and approved the final draft and are responsible for the content and similarity index of the manuscript.

Appendix A. Supplementary data

Supplementary data to this article can be found online at https://doi.org/10.1016/j.jtumed.2026.06.005.

References

1. Sallam M. Zoonotic diseases in the 21st century. **J Glob Health 2022**; 12:05001. https://doi.org/10.7189/jogh.12.05001.
2. Harapan H. Monkeypox outbreaks beyond Africa: a global concern. **Trav Med Infect Dis 2022**; 49:102348. https://doi.org/10.1016/j.tmaid.2022.102348.
3. Velavan TP. Monkeypox: a re-emerging zoonosis. **Trav Med Infect Dis 2022**; 49:102343. https://doi.org/10.1016/j.tmaid.2022.102343.
4. Morens DM, Fauci AS, Breman JG. Emerging zoonotic diseases: a global challenge. **Lancet Infect Dis 2022**; 22: 578−590. https://doi.org/10.1016/S1473-3099(22)00177-6.
5. Ahmed SF, Sohail MS, Quadeer AA, McKay MR. Vaccinia-Virus-Based Vaccines Are Expected to Elicit Highly Cross-Reactive Immunity to the 2022 Monkeypox Virus. **Viruses 2022 Sep 3**; 14(9): 1960. https://doi.org/10.3390/v14091960.
6. World Health Organization. *Mpox*; 2023 https://www.who.int/news-room/fact-sheets/detail/mpox. [Accessed 5 June 2026].
7. Pushpakom S, Iorio F, Eyers PA, Escott KJ, Hopper S, Wells A, et al. Drug repurposing: progress, challenges, and recommendations. **Nat Rev Drug Discov 2019**; 18: 41−58. https://doi.org/10.1038/nrd.2018.168.
8. Grosenbach DW. Tecovirimat for smallpox treatment. **N Engl J Med 2018**; 379: 44−53. https://doi.org/10.1056/NEJMoa1705688.
9. World Health Organization. *Monkeypox treatment guidelines*; 2022. https://www.who.int/teams/health-care-readiness/clinical-management-of-monkeypox. [Accessed 28 April 2023].
10. CDC. *Monkeypox treatment guidelines*. Centers for Disease Control and Prevention; 2022. https://www.cdc.gov/monkeypox/hcp/clinical-care/index.html. [Accessed 15 January 2026].
11. Alshahrani NZ. Monkeypox treatment guidelines in Saudi Arabia. **J Infect Public Health 2022**; 15: 901−905. https://doi.org/10.1016/j.jiph.2022.07.001.
12. Beigel JH, Tomashek KM, Dodd LE, Mehta AK, Zingman BS, Kalil AC, et al. Remdesivir for the treatment of COVID-19. **N Engl J Med 2020**; 383: 1813−1826. https://doi.org/10.1056/NEJMoa2007764.
13. Singhal S, Mehta J, Desikan R, Ayers D, Roberson P, Eddlemon P, et al. Thalidomide in multiple myeloma. **N Engl J Med 1999**; 341: 1565−1571. https://doi.org/10.1056/NEJM199911183412102.
14. Caly L, Druce J, Catton M. Ivermectin as a potential antiviral agent. **Antivir Res 2020**; 178:104787. https://doi.org/10.1016/j.antiviral.2020.104787.
15. Mehmood MA. Computational methods in drug discovery. **J Chem Inf Model 2014**; 54: 781−793. https://doi.org/10.1021/ci4006675.

16. Arasu MV, Vijayaragavan P, Purushothaman S, Rathi MA, Al-Dhabi NA, Gopalakrishnan VK, et al. Molecular docking of monkeypox (mpox) virus proteinase with FDA approved lead molecules. **Journal of Infection and Public Health 2023**; 16(5): 784−791. https://doi.org/10.1016/j.jiph.2023.03.004.
17. Preet G. Drug repurposing for monkeypox: a computational approach. **J Mol Graph Model 2022**; 115:108230. https://doi.org/10.1016/j.jmgm.2022.108230.
18. Bojkova D. Repurposing anticancer drugs for monkeypox treatment. **Antivir Res 2023**; 210:105487. https://doi.org/10.1016/j.antiviral.2023.105487.
19. Wang J, Shahed-AI-Mahmud M, Chen A, Li K, Tan H, Joyce R. An overview of antivirals against monkeypox virus and other orthopoxviruses. **J Med Chem 2023**; 66: 4468−4490.
20. Huang CY, Su SB, Chen KT. A review of epidemiology, diagnosis, and management of Mpox: the role of one health. **Global Health Med 2025**; 7: 1−12. https://doi.org/10.35772/ghm.2024.01072.
21. Kim S, Thiessen PA, Bolton EE, Chen J, Fu G, Gindulyte A, et al. PubChem substance and compound databases. **Nucleic Acids Res 2016**; 44: D1202−D1213.
22. Berman HM, Westbrook J, Feng Z, Gilliland G, Bhat TN, Weissig H, et al. The protein data bank. **Nucleic Acids Res 2000**; 28: 235−242.
23. Caillat C, Topalis D, Agrofoglio LA, Pochet S, Balzarini J, Deville-Bonne D, et al. Crystal structure of poxvirus thymidylate kinase: an unexpected dimerization has implications for antiviral therapy. **Proc Natl Acad Sci 2008**; 105: 16900−16905.
24. Silhan J, Klima M, Otava T, Skvara P, Chalupska D, Chalupsky K, et al. Discovery and structural characterization of monkeypox virus methyltransferase VP39 inhibitors reveal similarities to SARS-CoV-2 nsp14 methyltransferase. **Nat Commun 2023**; 14: 2259.
25. Peters JK, Tibble RW, Warminski M, Jemielity J, Gross JD. Structure of the poxvirus decapping enzyme D9 reveals its mechanism of cap recognition and catalysis. **Structure 2022**; 30: 721−732.e4.
26. Minasov G, Inniss NL, Shuvalova L, Anderson WF, Satchell KJ. Structure of the Monkeypox virus profilin-like protein A42R reveals potential functional differences from cellular profilins. **Acta Crystallogr F Struct Biol Commu 2022**; 78: 371−377.
27. Trott O, Olson AJ. AutoDock Vina: improving the speed and accuracy of docking with a new scoring function, efficient optimization, and multithreading. **J Comput Chem 2010**; 31: 455−461.
28. Milne GW. Software review of ChemBioDraw 12.0. **J Chem Inf Model 2010**; 50: 2053. https://pubs.acs.org/doi/full/10.1021/ci100385n.
29. Ortiz-Martínez Y. Bacterial co-infections in monkeypox. **Journal of Infection 2022**; 85(3): 345−350. https://doi.org/10.1016/j.jinf.2022.06.012.

How to cite this article: Gul S, Akhtar F, Rehman I, Shah M, Rashid U, Rauf A. Exploring drug repurposing for monkeypox virus: A structural and computational approach. J Taibah Univ Med Sc 2026;21(4):665−674.